*geologica**acta***

The Stillwater Complex chromitites: The response of chromite crystal chemistry to magma injection

D. LENAZ [1]   **G. GARUTI** [2]   **F. ZACCARINI** [2]   **R.W. COOPER** [3]   **F. PRINCIVALLE** [1]

[1] **Department of Mathematics and Geosciences**
Via Weiss 8, 34127 Trieste, Italy. Lenaz E-mail: lenaz@units.it

[2] **Department of Applied Geosciences and Geophysics**
Peter Tunner Strasse 5, 8700 Leoben, Austria

[3] **Department of Geology**
Lamar University, 77710 Beaumont TX, USA

┤ A B S T R A C T ├

Nineteen chromite crystals from the A, B, E, G, H, J and K chromitite layers of the Peridotite Zone of the Stillwater Complex (Montana, USA) have been studied by means of X-ray single crystal diffraction and microprobe analyses. The results show that samples from the basal A layer are quite different from the others showing very high oxygen positional parameter u (0.2633-0.2635) and Ti- contents (0.059-0.067apfu). Mg# values are within the range 0.21-0.23 while for the other chromites it is in the range 0.45-0.47. Moreover, for the other samples, according to the structural parameters, two groups have been identified. The first one comprises samples of layers B, E and G, the second includes H, J and K layer samples. It is supposed that high Fe^{2+} and Ti contents of A layer samples are due to the post-crystallization reaction with interstitial liquid. This fact allowed a very slow cooling rate as evidenced by the high u values. The fractionation of evolved magma from within the intrusion and pulse of a new magma bringing more chromium into the chamber lead to Cr- and Fe^{3+} -rich compositions and consequently to the increase of the cell edges. The decrease of u values seems to be related to the $Cr+Fe^{3+}$ and/or Al contents.

KEYWORDS | X-ray single crystal diffraction. Structural refinement. Cr-spinel. Stillwater.

INTRODUCTION

Cr-bearing spinels are widely regarded as important petrogenetic indicators. Several petrological studies have shown general relations between spinel chemistry, rock type and processes, and new understanding has been achieved of igneous/metamorphic events from analyses of spinel-bearing assemblages. In particular, the composition of chromite, in terms of chemical exchanges among Cr, Al, Mg, Fe^{2+}, Fe^{3+} and Ti, has become a common discriminating parameter to distinguish among podiform chromitites associated with residual mantle in sub-oceanic and sub-continental settings, stratiform chromitites in cratonic layered intrusions and chromite segregations in Ural-Alaskan type complexes (Irvine, 1967; Thayer, 1970; Sack, 1982; Dick and Bullen, 1984; Sack and

Ghiorso, 1991; Roeder, 1994; Stowe, 1994; Barnes and Roeder, 2001). Recently, the relations between chemistry and structural parameters in natural spinels have been considered by several authors, providing a new approach to the understanding of spinel crystallization mechanisms in magmatic and metamorphic environments (Della Giusta et al., 1986; Princivalle et al., 1989; Carraro, 2003; Bosi et al., 2004; Uchida et al., 2005; Lenaz et al., 2007, 2009, 2010). Structural data, essentially cell edge, a_0, and oxygen positional parameter, u, allow calculation of the cation distribution between the tetrahedral and octahedral sites in the spinel structure. The cell edge a_0 is apparently influenced by the spinel mineral chemistry, mainly the Al and Cr content. In contrast, the spinel oxygen coordinate u seems to be the most discriminating parameter, depending mainly on distribution of Mg and Al between tetrahedral and octahedral sites (Princivalle et al., 1989). Thus the u parameter is influenced by the degree of ordering of the spinel structure, becoming a powerful indicator of physical parameters prevailing in the chromite crystallizing system (Princivalle et al., 1989). More recent studies, anyway, argued that u parameter too can be related to the general chemistry (Lenaz et al., 2010). Studies have been previously performed on crystal chemistry of Cr-spinels from mantle nodules, sub-continental mantle massifs, ophiolites, kimberlites (Della Giusta et al., 1986; Princivalle et al., 1989; Carraro, 2003; Bosi et al., 2004; Uchida et al., 2005; Lenaz et al., 2007, 2009, 2010) and detrital in sedimentary environments (Carbonin et al., 1999; Lenaz and Princivalle, 1996, 2005; Lenaz et al., 2002)

Chemical structural studies on spinels from stratiform chromitites are limited to the case of the Bushveld layered Complex (Lenaz et al., 2007). The most relevant conclusion, in that case, was that small differences in oxygen positional parameter, u, were apparently related to variations in the cooling rate estimated from the filling and crystallization model of the Bushveld magma (Cawthorn and Walraven, 1998). Moreover, it was noticed that distinctive structural parameters were recorded for Cr-spinels having peculiar thermal histories such as those from the Merensky Reef and the Tweefontein pipe of the Bushveld Complex (Lenaz et al., 2007).

This study reports the results of a structural-chemical investigation of nineteen chromite crystals from seven chromitite layers located in the peridotite zone of the Stillwater Complex (Montana, USA). Major purposes of this work are: first, to increase the data base for Cr-spinels in chromitites from large, continental layered intrusions; second, to verify what relationships do exist between spinel structural parameters and chemical behaviour and petrogenetic models proposed for the Stillwater Complex.

GEOLOGICAL SETTING

The Stillwater Complex is located in southern Montana (USA) and consists of a more than 6km thick sequence of ultramafic to mafic layered rocks along the northern front of the Beartooth Mountains. A Sm-Nd isochron on mineral separates from a gabbronorite near the West Fork Adit portal gave a crystallization age of 2701±8Ma (DePaolo and Wasserburg, 1979). Nunes (1981) determined an age of 2713±3Ma on zircons from the Basal series and Premo et al. (1990) determined a U-Pb zircon age of 2705±4Ma for the dike/sill suite that is associated with the Basal Series, indicating that the sills are coeval with the main Complex emplaced at a depth of about 10-15km (McCallum, 1996).

The Complex is divided into three major stratigraphic series (Fig. 1) based on the mineralogy of the cyclic units: the Basal Series, the Ultramafic Series and the Banded Series. The Basal Series (average ~160m) separates the magmatic cumulates from footwall hornfels. It shows great variability in terms of lithologic sequence, however, predominantly consists of norite with minor peridotite, anorthosite and hornfels xenoliths, grading upwards into the basal bronzitite (McCallum, 2002). The appearance of extensive cumulus olivine marks the base of the Ultramafic Series that extends about 2000m in thickness (Mountain View section) up to the first appearance of plagioclase as a cumulus phase (Raedeke and McCallum, 1984). The Ultramafic Series is divided into a lower, Peridotite Zone, and upper, Bronzitite Zone. The Peridotite Zone, in its turn, is divided into six Megacyclic groups (numbered from the base as I to VI) comprising lithologically similar Multicyclic units of olivine–chromite–orthopyroxene cumulus layers, which are separated from each other by magmatic unconformities (Cooper, 1997, 2002). Towards the upper part of the Peridotite Zone, bronzite becomes the most abundant cumulus phase marking the transition to the Bronzitite Zone. The overlaying Banded Series (~4000m) comprises all rocks in which cumulus plagioclase is a major constituent, consisting of norite, gabbronorite, gabbro, troctolite and anorthosite (McCallum, 2002).

Successive massive chromite layers are restricted to the Peridotite zone being traditionally referred to as A (lowermost) through K (uppermost), of which layers G and H have been mined in the past (Campbell and Murck, 1993). They occur within olivine cumulates or olivine-bronzite cumulates, generally located close to the base of the Megacyclic groups. In the lowermost Megacyclic group I, a thick horizon enriched in hornfels inclusions has been observed in drill cores separating the chromitite layer A (Multicyclic unit A) from chromitites in the B Multicyclic unit (Cooper, 1997, 2002). Other chromitite layers occur in the Megacyclic groups IV (chromitite E), V (chromitites G, H, I), and VI (chromitites J and K).

GENETIC MODELS FOR THE STILLWATER COMPLEX

Mineralogical and isotopic variations through the sequence indicate that several magma types and multiple magma injections were responsible for the cumulate rocks present in the Stillwater Complex (Raedeke and McCallum, 1984; Lambert and Simmons, 1987; Lambert et al., 1989; Loferski et al., 1990; Campbell and Murck, 1993; Lipin, 1993; McCallum, 1996, 2002; Horan et al., 2001; Spandler et al., 2005).

Raedeke and McCallum (1984) showed that orthopyroxene compositions increased upsection from X_{Mg}=0.77 in the lowermosst Basal Series to 0.85 just above the B chromitite layer in the Ultramafic Series. These increases were interpreted to be due to the post-crystallization reaction with varying amounts of interstitial liquid, not to intrinsic differences in the compositions of successive pulses of magma. LREE (Light Rare Earth Elements) abundances in orthopyroxenes decrease upsection throughout the Peridotite Zone of the Ultramafic Series (Lambert and Simmons, 1987).

Recently, Horan et al., (2001) analyzed Re-Os isotopes of chromite separates within the Peridotite Zone. The chromites show variable initial Os isotopic compositions (γ_{Os} of +2.0 to +16.4) over the vertical extent of the Peridotite Zone, implicating at least two sources of Os. They argued the variations in γ_{Os} were caused by mixing of variable proportions of two magmas having different Os isotopic compositions. One of the magmatic components was a more primitive magma with a nearly chondritic Os isotopic composition. The other magma had a radiogenic Os isotopic composition as a result of the assimilation of crustal material. The gradual decrease in the initial γ_{Os} values of the chromite layers with increasing stratigraphic height implies a decreasing relative contribution from the contaminated magma throughout the development of the Peridotite Zone.
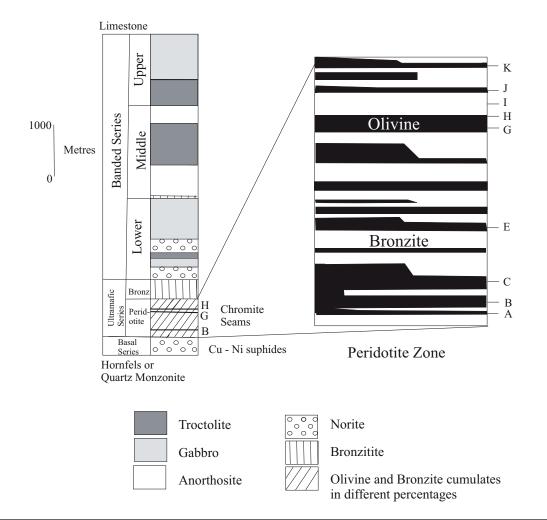

FIGURE 1 | Generalized stratigraphic column of the Stillwater Complex, Montana; after Raedeke and McCallum (1984), Campbell and Murck (1993) and McCallum (1996).

Spandler et al. (2005) described multiphase silicate inclusions trapped within chromite grains from the G chromitite seam. Silicate inclusions within chromite are interpreted to represent melt trapped during chromite growth and hence provide information on their formation (Kamenetsky, 1996; Kamenetsky et al., 2001; Danyushevsky et al., 2004; Shimizu et al., 2009). These inclusions have variable quench textures and chemical compositions that are consistent with variable degrees of mixing between a high-Mg basaltic parental magma and a Na-rich trondhjemitic melt derived from partial melting of mafic or metasedimentary country rocks. The model provided by Spandler et al. (2005) consequently outlined the ponding of a new pulse of primitive magma (temperature higher than 1400°C) at the roof of the Stillwater magma chamber, followed by localized partial melting and assimilation of country rock. Mixing between the trondhjemite and parent magma at the roof of the magma chamber led to localized hybridization and rapid cooling of the melt. The newly formed hybrid melts become oversaturated in chromite, leading exclusively to chromite crystallization. Rapid chromite growth promoted entrapment of samples of the hybrid magma. Rapid crystallization and cooling would also promote the convective overturn of the parental magma at the roof of the chamber (Marsh, 1988), allowing large volumes of primitive magma to interact with the country rock over a relatively short time, and hence, extensive chromite accumulation.

SAMPLE PROVENANCE AND ANALYTHICAL METHODS

The investigated samples were collected in Mountain View section (layers A, B, G, H, HWH) and from the Benbow mine (layers E, J and K). Samples SWA1 and SWA1A are from layer A, SWLB2, SWLB2A, SW4B, SW4BA from layer B, SWE1, SWE1A from layer E, STW6A and SW6A from layer G, SWH2, SWH2A from layer H, SWHWH1A and SWHWH1B from the Hanging Wall chromitite of layer H, SWJ1, SWJ1A and SWJ1B from layer J, SWK2 and SWK2A from layer K.

X-Ray single crystal diffraction

Nineteen single crystals of chromite were analysed from chromitite layers A through K. X-ray diffraction data were recorded on an automated KUMA-KM4 (K-geometry) diffractometer, using MoK radiation, monochromatised by a flat graphite crystal. Data collection was made, according to Della Giusta et al. (1996), up to 55° of in the -2 scan mode, scan width 1.8°2θ, counting time from 20 to 50 seconds depending on the peak intensity standard deviation. Twenty-four equivalent reflections of (12 8 4) peak, at about 80° of 2θ, were accurately centred at both sides of 2θ, and the α_1 peak baricentre was used for cell

parameter determination. Corrections for absorption were performed according to North et al. (1968). Structural refinement using the SHELX-97 program (Sheldrick, 1997) was carried out against Fo^2_{hkl} in the Fd-3m space group (with origin at -3m), since no evidence of different symmetry appeared. Refined parameters were scale factor, oxygen positional parameter (u), tetrahedral and octahedral site occupancies, and thermal displacement parameters (U). Scattering factors were taken from Prince (2004) and Tokonami (1965). Two neutral scattering curves, Mg vs. Fe in T site and Cr vs. Al in M site, were assigned to sites involved in isomorphous replacements, with the constraints of full site occupancy and equal displacement parameters, whereas oxygen was considered to be in a partly ionised state (70%). No constraints were imposed by chemical analyses. Crystallographic data are listed in Table 1.

Chemical microanalyses and cation partitioning

Ten to fifteen spot chemical analyses were performed on the same crystals (SW6A crystal being lost during polishing) used for X-ray data collection using a CAMECA SX50 electron microprobe operating at 15kV and 15nA, 10s counting time for peak and 5sec for total background. Natural and synthetic oxide standards (MgO, FeO, MnO, ZnO, NiO, Al_2O_3, Cr_2O_3, TiO_2 and SiO_2) were used. The raw data were reduced with PAP-type correction software provided by CAMECA. Chemical data are listed in Table I (available at www.geologica-acta.com). Fe_2O_3 was calculated according to stoichiometry.

Cation distribution (Table I) between T and M sites were obtained with the method described by Carbonin et al. (1996) and Lavina et al. (2002), in which cations are assigned to the tetrahedral and octahedral sites of the structure according to their scattering power and a set of bond distances optimised for spinel structure. Structure parameters are calculated as a function of the atomic fractions at the two sites and fitted to the observed ones. Site atomic fractions are calculated by minimising the function F(x) (Table 1) which takes into account the mean of the square differences between calculated and observed parameters, divided by their square standard deviations.

Chemical analyses were also obtained on other crystals from the A, B, G, H and J layers. In Figure 2, the Cr# (Cr/Cr+Al) vs. Fe# ($Fe^{2+}/Fe^{2+}+Mg$) of analysed crystals are plotted.

RESULTS

Structural analyses show that the cell edge, a_0, of the studied samples spans between 8.2739 (2) and 8.2990 (2) Å. In Fig. 3, where cell edges are shown against their

TABLE 1 | Results of structure refinement. MV: Mountain View section; BM: Benbow Mine; a0: cell parameter (Å); u: oxygen positional parameter; T-O and M-O: tetrahedral and octahedral bond lenghts (Å), respectively; m.a.n.: mean atomic number; U(M), U(T), U(O): displacement parameters for M site, T site and O; R1 all (%), wR2 (%), GooF as defined in Sheldrick (1997). F(x): minimization factor which takes into account the mean of the square differences between calculated and observed parameters, divided by their square standard deviations. Estimated standard deviations in brackets. *F(x) not determined due to the loss of crystal during polishing

Sample	SWA1	SWA1A	SWLB2	SWLB2A	SW4B	SW4BA	SWE1	SWE1A	STW6A	SW6A
Layer	A	A	B	B	B	B	E	E	G	G
Locality	MV	MV	MV	MV	MV	MV	BM	BM	MV	MV
a_0	8.2917 (2)	8.2898 (2)	8.2739 (2)	8.2746 (3)	8.2831 (1)	8.2865 (1)	8.2951 (4)	8.2979 (1)	8.2990 (2)	8.2988 (2)
u	0.26347(7)	0.26330(7)	0.26301(15)	0.26291(6)	0.26287(7)	0.26287(6)	0.26267(14)	0.26262(7)	0.26255(6)	0.26260 (7)
T-O	1.989	1.987	1.979	1.977	1.978	1.978	1.976	1.978	1.978	1.978
M-O	1.968	1.968	1.966	1.968	1.970	1.970	1.975	1.975	1.976	1.976
m.a.n. T	23.5 (1)	22.8 (3)	19.3 (1)	19.3 (3)	19.1 (2)	19.2 (2)	19.4 (7)	19.3 (3)	18.4 (2)	
m.a.n. M	19.5 (1)	19.4 (3)	19.9 (2)	19.7 (3)	19.9 (3)	20.0 (2)	21.4 (9)	21.0 (4)	21.0 (2)	
U (M)*10^5	509(7)	473(11)	920(18)	404(8)	463(11)	438(7)	566(22)	396(11)	356(8)	441 (8)
U (T)*10^5	822(12)	744(13)	1132(25)	623(13)	682(16)	672(13)	677(32)	576(17)	541(14)	670 (15)
U (O)*10^5	772(18)	744(23)	1116(32)	633(14)	700(7)	672(14)	687(40)	578(19)	570(15)	663 (18)
R1	2.14	1.87	3.81	2.53	2.57	2.04	5.87	2.43	1.66	2.04
wR2	3.44	3.19	5.47	4.38	4.78	3.77	8.72	4.54	4.10	3.31
GooF	1.330	1.180	1.063	1.436	1.275	1.327	1.274	1.411	1.143	1.345
F(x)	0.026	0.174	0.379	0.507	0.131	0.295	0.109	0.187	0.073	n.d.*

Sample	SWH2	SWH2A	SWHWH1B	SWHWH1A	SWJ1A	SWJ1B	SWJ1	SWK2	SWK2A
Layer	H	H	HWH	HWH	J	J	J	K	K
Locality	MV	MV	MV	MV	BM	BM	BM	BM	BM
a_0	8.2781 (1)	8.2796 (2)	8.2772 (2)	8.27412 (8)	8.2759 (1)	8.2785 (2)	8.2786 (1)	8.2880 (2)	8.2899 (2)
u	0.26246(10)	0.26276(7)	0.26306(6)	0.26306(6)	0.26308(13)	0.26288(6)	0.26270(7)	0.26272(5)	0.26278(7)
T-O	1.973	1.976	1.979	1.979	1.979	1.977	1.975	1.977	1.978
M-O	1.971	1.970	1.967	1.966	1.967	1.969	1.970	1.972	1.972
m.a.n. T	17.9 (2)	17.9 (2)	19.5 (2)	19.7 (2)	18.7 (3)	18.9 (1)	18.6 (2)	20.2 (3)	19.3 (3)
m.a.n. M	20.2 (2)	20.3 (2)	19.6 (3)	19.8 (3)	20.0 (3)	19.9 (1)	19.9 (2)	20.2 (3)	20.5 (5)
U (M)*10^5	612(10)	443(8)	433(9)	470(9)	628(17)	402(6)	470(7)	308(9)	398(13)
U (T)*10^5	827(19)	672(14)	673(12)	693(14)	850(27)	647(12)	689(14)	510(13)	603(16)
U (O)*10^5	844(23)	641(17)	656(18)	658(19)	904(30)	624(15)	700(15)	529(15)	610(22)
R1	2.23	1.95	1.63	1.77	3.77	1.83	1.98	2.72	2.65
wR2	4.73	3.42	2.73	3.02	9.19	3.21	3.65	4.71	4.69
GooF	0.915	1.295	1.215	1.199	1.237	1.306	1.289	1.495	1.423
F(x)	0.102	1.270	0.396	0.175	0.126	0.602	0.070	0.242	0.075

stratigraphic position, a linear increase from sample SW4B (B layer) to sample STW6A (G layer) is present.

Oxygen positional parameter u spans from 0.26256 (15) to 0.26347 (7). Figure 4 shows the behaviour of u along the stratigraphic position. Chemical analyses (Table I) show that Cr# spans from 0.54 to 0.68, while Mg# is within the range 0.45-0.57. The A layer is characterized by significantly lower Mg#=0.21-0.23, at Cr# values of 0.54-0.56. Cation distribution shows that the studied crystals are well ordered, i.e. Mg and Al essentially in T and M sites, respectively (Table I), in fact the highest content of Al in the T site is 0.015 atoms per formula unit (apfu). This fact is obviously reflected in the oxygen positional parameter u, that is always higher than 0.2625 as Princivalle et al. (1989) showed that ordered spinels commonly show u values higher than 0.2625.

As regards the T site, the content of Mg and Fe^{2+} is rather similar and is about 0.5 apfu apart from sample SWA1 and SWA1A. These samples show about 0.77 Fe^{2+} apfu and 0.17 Mg apfu (Fig. 5A). In M site, Cr is the more
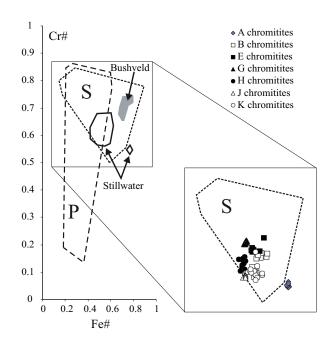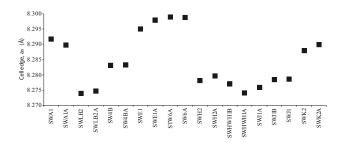

FIGURE 2 | Plot of Cr# vs. Fe# for chromite samples from the Stillwater Complex. S: stratiform chromitites; P: peridotitic chromitites.

FIGURE 3 | Cell edge variations along the stratigraphic column. Estimated standard deviations are within the symbols.

FIGURE 4 | Oxygen positional parameter variations along the stratigraphic column.

abundant cation representing about half of the site cations. Al is comprised between 0.56 and 0.79 apfu (Fig. 5B). Fe^{3+} behaviour seems to be quite peculiar. It is more or less constant (0.09apfu) in A and B layers, fairly high in E and G layers (0.20apfu), and shows a linear increase from H to K layers (0.09 to 0.20apfu) (Fig. 5C). Titanium is very high in A layer (0.057-0.069apfu) and almost constant in all the other layers (0.010-0.025apfu) (Fig. 5C). There is a positive relation between M-O bond length and cell edge while T-O distances are more or less constant with regard to the cell edge. A T-O bond distance larger than the M-O bond distance suggests the presence of prevalent large cations in the T site.

DISCUSSION

There are several significant observations that can be made based on the results described above.

Firstly, there is the anomalous character of samples from the A layer. They are very Fe- and Ti-rich with respect to others and present very high u values. Fe- and Ti-rich chromite is generally recognized as having formed later than the chromitites due to the action of a late intercumulus melt (Kinloch and Peyerl, 1990; Scoon and Mitchell, 1994). Raedeke and McCallum (1984) effectively attributed minor variations in the lowermost cyclic unit of Stillwater to post-crystallization reaction with interstitial liquid possibly causing an enrichment in Fe and Ti. Princivalle et al. (1989) noticed that there is a positive correlation between cell edge and Cr content in Cr-spinels from mantle xenoliths (Fe^{3+} is negligible in nodule Cr-spinels). In the Stillwater samples this correlation is not evident, it is more evident if $Cr+Fe^{3+}$ are compared with cell edges (Fig. 6) as evidenced by Lenaz et al. (2010) for Cr-spinels from Ronda peridotites. Samples from A layer plot off the trend, in fact the cell edges of SWA1 and SWA1A are very high with respect to $Cr+Fe^{3+}$ content. This is possibly caused by the very large T-O bond distance of the two samples due to the presence of a high Fe^{2+} content in the T site (T-O bond length for Mg is 1.965 Å, 1.997 Å for Fe^{2+}; Lenaz et al.,
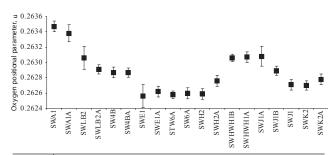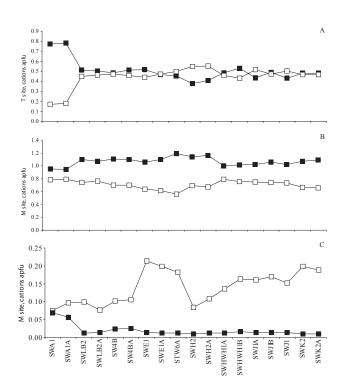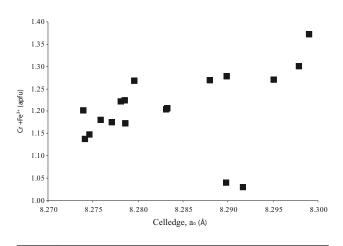
2004a). The higher T-O bond length also causes the u value increase. Figure 7 shows the behaviour of M-O vs. T-O bond distances in chromites from layered intrusions (Great Dyke and Finero, Lenaz unpublished data; Bushveld, Lenaz et al., 2007; and Stillwater, this study). Chromites from layered intrusions do not usually show u values higher than about 0.2630 so that the higher u value of A (0.2633-0.2635) could be the effect of a "recrystallization" of chromites due to interaction with trapped intercumulus liquid that caused Fe^{2+} and Ti enrichment (Fig. 4).

The second noteworthy observation is a possible division of the studied samples into two groups. The first group is represented by samples from layers B to G featuring an increase of cell edge, Cr and Fe^{3+} contents

FIGURE 5 | Cation (apfu) variations along the stratigraphic column. A) T site. Full square: Fe^{2+}; open square: Mg. B) M site. Full square: Cr; open square: Al. C) M site: Full square: Ti; open square: Fe^{3+}.

FIGURE 8 | Oxygen positional parameter, u, vs. Cr + Fe^{3+} (apfu; open square) and Al (apfu; full square).

and a decrease of the u values and Al content. After an initial breakdown, mainly of the cell parameter, this behaviour is similar also for the samples above the G layer (H to K). The decrease of the crustal assimilation, as outlined by the γ_{Os} values, the fractionation of evolved magma from within the intrusion and pulse of a new magma bringing more chromium into the chamber probably leads to Cr- and Fe^{3+} -rich compositions (B to G layers). For all these layers the main silicate cumulate mineral is olivine. Within and above the H multicyclic unit the main cumulate mineral is bronzite. This may have been due to a combination of fractional crystallization within the chamber, the addition of new magma and a component of high-silica melted roof-rock (Horan et al., 2001). Small variations in γ_{Os} between different chromite occurrences reflects the petrologic requirement that chromite layers crystallize from
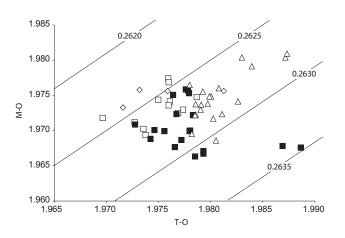
slightly different proportions of the magmas, compared to chromite from olivine- and orthopyroxene-rich layers. Changes in chromite chemistry reflect variations in mixing proportions. However the evolutionary trend is the same as outlined for the first group, i.e. pulse of a new magma bringing more chromium into the chamber leads to Cr- and Fe^{3+} -rich compositions. Spandler et al. (2005) suggested rapid cooling for the G layer due to the localized hybridization between the trondhjemitic melt formed when hot primitive magma enters the chamber, melting its roof and parent magma. Based on this interpretation, the u values should depend on the interaction between the primitive magma and the residual melts and their relative temperature and cooling rates. In fact, a rapid cooling causes a relative disorder in the cation distribution among the sites and, consequently, low u values as shown by sample SW6A from the G layer.

A second explanation is what we describe as a "cover" effect. The new impulse of magma covers the existing layers and prevents the heat loss so that the older layers are warmed for a longer period and consequently the cation site exchange continues for a longer time.

The third explanation is the simplest and implies that high-Cr content could inhibit the cation exchange of Al and Mg between T and M sites (Lenaz et al., 2004b). In such a model the u values are only a function of Cr+Fe^{3+} and/or Al content in the M site (Fig. 8), meaning it depends only on the chemistry of the chromite grains as can be seen in Lenaz et al. (2010) for Cr-spinels from Ronda mantle peridotites.

FIGURE 7 | T-O vs. M-O bond length (Å). Full square: this study; open triangle: Bushveld Complex (Lenaz et al., 2007) and Great Dyke Complex (Lenaz et al., unpublished data) layered complexes; open square: Finero massive chromites (Lenaz et al., unpublished data). Lines represent equal u values.
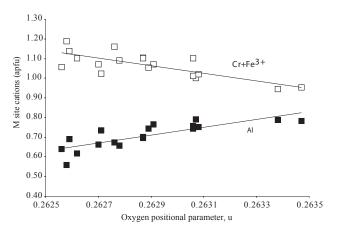
ACKNOWLEDGMENTS

REFERENCES

Barnes, S.J., Roeder, P.L., 2001. The range of spinel compositions in terrestrial mafic and ultramafic rocks. Journal of Petrology, 42, 2279-2302.

Bosi, F., Andreozzi, G.B., Ferrini, V., Lucchesi, S., 2004. Behavior of cation vacancy in kenotetrahedral Cr-spinels from Albanian eastern belt ophiolites. American Mineralogist, 89, 1367-1373.

Campbell, I.H., Murck, B.W., 1993. Petrology of the G and H chromitite zones in the Mountain View area of the Stillwater Complex, Montana. Journal of Petrology, 34, 291-316.

Carbonin, S., Menegazzo, G., Lenaz, D., Princivalle, F., 1999. Crystal chemistry of two detrital Cr -spinels with unusual low values of oxygen positional parameter: Oxidation mechanism and possible clues to their origin. Neues Jahrbuch für Mineralogie Monatshefte, 359-371.

Carbonin, S., Russo, U., Della Giusta, A., 1996. Cation distribution in some natural spinels from X-ray diffraction and Mössbauer spectroscopy. Mineralogical Magazine, 60, 355-368.

Carraro, A., 2003. Crystal chemistry of Cr-spinels from a suite of spinel peridotite mantle xenoliths from the Predazzo Area (Dolomites, Northern Italy). European Journal of Mineralogy, 15, 681-688.

Cawthorn, R.G., Walraven, F., 1998. Emplacement and crystallization time for the Bushveld Complex. Journal of Petrology, 39, 1669-1687.

Cooper, R.W., 1997. Magmatic Unconformities and Stratigraphic Relations in the Peridotite zone, Stillwater Complex, Montana. Canadian Journal of Earth Sciences, 34, 407-425.

Cooper, R.W., 2002. Stratigraphy and Chromite Mineralization of the Peridotite Zone, Stillwater Complex, Montana. In: Bordreau, A.E., (ed.). Stillwater Complex, Geology and Guide. Billings, 21-25 July 2002, 9th International Platinum Symposium, D1-68.

Danyushevsky, L.V., Leslie, R.A.J., Crawford, A.J., Durance, P., 2004. Melt inclusions in primitive olivine phenocrysts. The role of localized reaction processes in the origin of anomalous compositions. Journal of Petrology, 45, 2531-2553.

Della Giusta, A., Carbonin, S., Ottonello, G., 1996. Temperature-dependant disorder in a natural Mg - Al - Fe^{2+} - Fe^{3+} - spinel. Mineralogical Magazine, 60, 603-616.

Della Giusta, A., Princivalle, F., Carbonin, S., 1986. Crystal chemistry of a suite of natural Cr-bearing spinels with 0.15 < Cr < 1.07. Neues Jahrbuch für Mineralogie Abhlandungen, 155, 319-330.

DePaolo, D.J., Wasserburg, G.J., 1979. Sm-Nd age of the Stillwater Complex and the mantle evolution curve for neodymium. Geochimica et Cosmochimica Acta, 43, 999-1008.

Dick, H.J.B., Bullen, T., 1984. Chromian spinel as a petrogenetic indicator in abyssal and alpine-type peridotites and spatially associated lavas. Contributions to Mineralogy and Petrology, 86, 54-76.

Horan, M.F., Morgan, J.W., Walker, R.J., Cooper, R.W., 2001. Re-Os isotopic constraints on magma mixing in the Peridotite Zone of the Stillwater Complex, Montana, USA. Contributions to Mineralogy and Petrology, 141, 446-457.

Irvine, T.N., 1967. Chromian spinel as a petrogenetic indicator. Part 2. Petrologic applications. Canadian Journal of Earth Sciences, 4, 71-103.

Kamenetsky, V.S., 1996. Methodology for the study of melt inclusions in Cr-spinel, and implications for parental melts of MORB from FAMOUS area. Earth and Planetary Science Letters, 142, 479-486.

Kamenetsky, V.S., Crawford, A.J., Meffre, S., 2001. Factors controlling chemistry of magmatic spinel: an empirical study of associated olivine, Cr-spinel and melt inclusions from primitive rocks. Journal of Petrology, 42, 655-671.

Kinloch, E.D., Peyerl, W., 1990. Platinum-group minerals in various rock types of the Merensky reef: genetic implications. Economic Geology, 85, 537-555.

Lambert, D.D., Morgan, J.W., Walker, R.J., Shirey, S.B., Carlson, R.W., Zientek, M.L., Koski, M.S., 1989. Rhenium-Osmium and Samarium-Neodymium isotopic systematics of the Stillwater Complex. Science, 244, 1169-1174.

Lambert, D.D., Simmons, E.C., 1987. Magma evolution in the Stillwater Complex, Montana: I. Rare-earth evidence for the formation of the Ultramafic Series. American Journal of Science, 287, 1-32.

Lavina, B., Salviulo, G., Della Giusta, A., 2002. Cation distribution and structure modelling of spinel solid solutions. Physics and Chemistry of Minerals, 29, 10-18.

Lenaz, D., Princivalle, F. 1996. Crystal-chemistry of detrital chromites in sandstones from Trieste (NE Italy). Neues Jahrbuch für Mineralogie Monatshefte, 429-434.

Lenaz, D., Carbonin, S., Gregoric, M., Princivalle, F. 2002. Crystal chemistry and oxidation state of one euhedral Cr-spinel crystal enclosed in a bauxite layer (Trieste Karst: NE Italy): Some considerations on its depositional history and provenance. Neues Jahrbuch für Mineralogie Monatshefte, 193-206.

Lenaz, D., Skogby, H., Princivalle, F., Hålenius, U., 2004a. Structural changes and valence states in the MgCr$_2$O$_4$ - FeCr$_2$O$_4$ solid solution series. Physics and Chemistry of Minerals, 31, 633-642.

Lenaz, D., Andreozzi, G.B., Mitra, S., Bidyananda, M., Princivalle, F., 2004b. Crystal chemical and ^{57}Fe Mössbauer study of chromite from the Nuggihalli schist belt (India). Mineralogy and Petrology, 80, 45-57.

Lenaz, D., Princivalle, F., 2005. The crystal chemistry of detrital chromian spinel from the Southeastern Alps and Outer Dinarides: the discrimination of supplies from areas of similar tectonic setting? Canadian Mineralogist, 43, 1305-1314.

Lenaz, D., Braidotti, R., Princivalle, F., Garuti, G., Zaccarini, F., 2007. Crystal chemistry and structural refinement of

chromites from different chromitite layers and xenoliths of the Bushveld Complex. European Journal of Mineralogy, 19, 599-609.

Lenaz, D., Logvinova, A.M., Princivalle, F., Sobolev, N.V., 2009. Structural parameters of chromite included in diamond and kimberlites from Siberia: a new tool for discriminating ultramafic source. American Mineralogist, 94, 1067-1070.

Lenaz, D., De Min, A., Garuti, G., Zaccarini, F., Princivalle, F., 2010. Crystal chemistry of Cr-spinels from the lherzolite mantle peridotite of Ronda (Spain). American Mineralogist, 95, 1323-1328. doi: 10.2138/am.2010.3545

Lipin, B.R., 1993. Pressure increases, the formation of cromite seams, and the development of the Ultramafic Series in the Stillwater Complex, Montana. Journal of Petrology, 34, 955-974.

Loferski, P.J., Lipin, B.R., Cooper, R.W., 1990. Petrology of chromite-bearing rocks from the lowermost cyclic units in the Stillwater Complex, Montana. USGS Bulletin 1674-E, 1-28.

Marsh, B.D., 1988. Crystal capture, sorting and retention in convecting magma. Geological Society of America Bulletin, 100, 1720-1737.

McCallum, I.S., 1996. The Stillwater Complex. In: Cawthorn, R.G. (ed.). Layered intrusions, Amsterdam, Elsevier Science, 441-483.

McCallum, I.S., 2002. The Stillwater Complex: A review of the geology. In: Boudreau, A.E., (ed.). Stillwater Complex, Geology and Guide. Billings, 21-25 July 2002, 9th International Platinum Symposium, A1-25.

North, A.C.T., Phillips, D.C., Scott-Mattews, F., 1968. A semi-empirical method of absorption correction. Acta Crystallographica, A24, 351-352.

Nunes, P.D., 1981. The age of the Stillwater Complex; a comparison of U-Pb zircon and Sm-Nd isochron systematics. Geochimica et Cosmochimica Acta, 45, 1961-1963.

Premo, W.R., Helz, R.T., Zientek, M.L., Langston, R.B., 1990. U-Pb and Sm-Nd ages for the Stillwater Complex and its associated sill and dykes, beartooth Mountains, Montana: identification of a parent magma? Geology, 18, 1065-1068.

Prince, E., 2004. International Tables for X-ray Crystallography. Volume C: Mathematical, physical and chemical tables.

Dordrecht (The Netherlands), 3rd edition Sprinter, 1000pp.

Princivalle, F., Della Giusta, A., Carbonin, S., 1989. Comparative crystal chemistry of spinels from some suits of ultramafic rocks. Mineralogy and Petrology, 40, 117-126.

Raedeke, L.D., McCallum, I.S., 1984. Investigations in the Stillwater Complex: Part II. Petrology and petrogenesis of the Ultramafic Series. Journal of Petrology, 25, 395-420.

Roeder, P.L., 1994. Chromite: from the Fiery rain of chondrules to the Kilauea Iki lava lake. Canadian Mineralogist, 32, 729-746.

Sack, R.O., 1982. Spinels as petrogenetic indicators: Activity-composition relations at low pressures. Contributions to Mineralogy and Petrology, 79, 169-186.

Sack, R.O., Ghiorso, M.S., 1991. Chromian spinels as petrogenetic indicators: Thermodynamics and petrological applications. American Mineralogist, 76, 827-847.

Scoon, R.N., Mitchell, A.A., 1994. Discordant iron-rich ultramafic pegmatites in the Bushveld Complex and their relationship to iron-rich intercumulus and residual liquids. Journal of Petrology, 35, 881-917.

Sheldrick, G.M., 1997. SHELX-97. Program for crystal structure refinement. Germany, University of Gottingen, Gottingen.

Shimizu, K., Shimizu, N., Komiya, T., Suzuki, K., Maruyama, S., Tatsumi, Y., 2009. CO_2-rich komatiitic melt inclusions in Cr-spinels within beach sand from Gorgona Island, Colombia. Earth and Planetary Science Letters, 288, 33-43.

Spandler, C., Mavrogenes, J., Arculus, R., 2005. Origin of chromitites in layered intrusions: Evidence from chromite-hosted melt inclusions from the Stillwater Complex. Geology, 33, 893-896.

Stowe, C.W., 1994. Compositions and tectonic settings of chromite deposits through time. Economic Geology, 89, 528-546.

Thayer, T.P., 1946. Preliminary chemical correlation of chromite with the containing rocks. Economic Geology, 41, 202-217.

Tokonami, M., 1965. Atomic scattering factor for O^{-2}. Acta Crystallographica, 19, 486.

Uchida, H., Lavina, B., Downes, R.T., Chesley, J., 2005. Single-crystal X-ray diffraction of spinels from the San Carlos Volcanic Field, Arizona: Spinel as a geothermometer. American Mineralogist, 90, 1900-1908.

ELECTRONIC APPENDIX

TABLE I | Mean chemical analyses (10 to 15 spot analyses for each crystal) and cation distribution in T and M sites of the analysed chromites. Cr#: Cr/(Cr+Al); Mg#: Mg/(Mg+Fe2+). Estimated standard deviations in brackets

Samples	SWA1	SWA1A	SWLB2	SWLB2A	SW4B	SW4BA	SWE1	SWE1A	STW6A
Layer	A	A	B	B	B	B	E	E	G
Locality	MV	MV	MV	MV	MV	MV	BM	BM	MV
MgO	4.34(46)	5.00(24)	10.10(15)	9.91(20)	10.13(11)	10.11(13)	9.98(15)	9.95(18)	10.91(27)
Al_2O_3	20.04(27)	20.41(22)	20.55(20)	20.35(14)	18.99(18)	18.38(20)	16.88(15)	16.21(24)	14.78(17)
SiO_2	0.09(2)	0.85(6)	0.07(2)	1.05(11)	0.18(4)	0.76(5)	0.80(3)	0.19(8)	0.23(2)
TiO_2	2.72(41)	2.33(29)	0.55(4)	0.58(2)	0.99(4)	1.06(4)	0.55(4)	0.54(3)	0.51(3)
Cr_2O_3	36.28(43)	36.23(37)	44.54(49)	42.47(35)	43.58(57)	43.77(49)	41.49(47)	43.22(41)	46.65(43)
MnO	0.35(5)	0.34(5)	0.31(5)	0.27(4)	0.23(6)	0.24(7)	0.25(3)	0.25(4)	0.22(4)
FeO	34.30(57)	33.50(57)	24.47(30)	24.09(32)	24.60(22)	22.63(36)	28.64(34)	29.22(40)	25.79(44)
NiO	0.17(8)	0.15(5)	0.00	0.00	0.12(5)	0.12(6)	0.00	0.00	0.11(4)
ZnO	0.23(9)	0.00	0.00	0.00	0.00	0.04	0.00	0.00	0.00
Σ	98.56	98.83	100.66	98.76	98.86	97.11	98.61	99.16	99.24
FeO	30.04(57)	30.04(57)	20.41(30)	21.39(32)	20.06(22)	18.98(36)	20.44(34)	19.94(40)	18.04(44)
Fe_2O_3	4.73	3.84	4.51	3.00	5.04	4.05	9.10	10.31	8.61
Σ	99.04	99.22	101.07	99.06	99.36	97.51	99.52	100.64	100.11
T Site									
Al	0.005	0.000	0.015	0.000	0.012	0.000	0.002	0.000	0.005
Fe^{2+}	0.772	0.783	0.512	0.503	0.484	0.512	0.517	0.469	0.453
Fe^{3+}	0.040	0.000	0.009	0.000	0.019	0.000	0.008	0.042	0.026
Mg	0.170	0.180	0.452	0.462	0.473	0.459	0.441	0.474	0.502
Mn	0.010	0.010	0.008	0.008	0.007	0.007	0.007	0.007	0.006
Si	0.003	0.027	0.003	0.028	0.006	0.023	0.026	0.007	0.008
Σ	1.000	1.000	1.000	1.000	1.000	1.000	1.000	1.000	1.000
M Site									
Al	0.782	0.789	0.744	0.766	0.703	0.697	0.640	0.618	0.558
Fe^{2+}	0.063	0.045	0.020	0.065	0.054	0.043	0.036	0.063	0.032
Fe^{3+}	0.076	0.097	0.099	0.077	0.102	0.105	0.213	0.199	0.183
Mg	0.051	0.066	0.020	0.006	0.011	0.024	0.040	0.005	0.022
Cr	0.954	0.944	1.103	1.072	1.103	1.101	1.058	1.102	1.190
Ti	0.069	0.057	0.013	0.014	0.024	0.025	0.014	0.013	0.013
Ni	0.005	0.004	0.000	0.000	0.003	0.004	0.000	0.000	0.003
Σ	2.000	2.000	2.000	2.000	2.000	2.000	2.000	2.000	2.000
Cr#	0.55	0.54	0.59	0.58	0.61	0.61	0.62	0.64	0.68
Mg#	0.21	0.23	0.47	0.45	0.47	0.47	0.47	0.47	0.52

TABLE I | Continued

Samples	SWH2	SWH2A	HWH1B	HWH1A	SWJ1A	SWJ1B	SWJ1	SWK2	SWK2A
Layer	H	H	HWH	HW	J	J	J	K	K
Locality	MV	MV	MV	MV	BM	BM	BM	BM	BM
MgO	12.24(25)	12.18(16)	9.75(22)	9.97(39)	11.16(14)	11.31(29)	11.27(14)	10.01(11)	9.89(12)
Al_2O_3	19.15(15)	18.31(39)	20.61(19)	21.62(60)	20.26(12)	19.83(19)	20.19(23)	17.99(21)	17.60(21)
SiO_2	0.08(1)	0.23(2)	0.23(3)	0.11(1)	0.16(2)	0.98(27)	0.11(3)	0.21(02)	0.11(3)
TiO_2	0.43(6)	0.52(3)	0.66(4)	0.52(3)	0.57(4)	0.58(3)	0.58(2)	0.39(05)	0.41(2)
Cr_2O_3	45.99(39)	46.23(50)	40.38(37)	40.07(67)	41.15(56)	40.27(52)	40.80(59)	42.50(53)	42.88(61)
MnO	0.27(4)	0.24(5)	0.31(9)	0.31(3)	0.28(5)	0.28(4)	0.25(2)	0.27(4)	0.28(4)
FeO	21.39(38)	20.70(22)	27.38(40)	26.40(31)	25.88(52)	25.27(25)	25.33(26)	28.06(46)	27.67(40)
NiO	0.16(3)	0.13(5)	0.00	0.14(5)	0.15(5)	0.13(6)	0.17(4)	0.12(2)	0.15(7)
ZnO	0.00	0.00	0.00	0.00	0.00	0.00	0.00	0.00	0.00
Σ	99.73	98.57	99.33	99.17	99.64	98.68	98.71	99.58	99.03
FeO	16.44(38)	16.33(22)	20.89(40)	20.22(31)	18.52(52)	18.96(25)	17.99(26)	19.85(46)	19.63(40)
Fe_2O_3	5.50	4.85	7.21	6.85	8.17	7.01	8.15	9.12	8.93
Σ	100.28	99.06	99.34	99.85	100.46	99.38	99.35	100.49	99.92
T Site									
Al	0.015	0.015	0.015	0.009	0.000	0.000	0.015	0.015	0.011
Fe^{2+}	0.378	0.411	0.530	0.488	0.436	0.493	0.431	0.483	0.483
Fe^{3+}	0.046	0.010	0.010	0.030	0.032	0.000	0.040	0.021	0.028
Mg	0.551	0.554	0.432	0.461	0.519	0.474	0.503	0.467	0.466
Mn	0.007	0.007	0.007	0.008	0.008	0.008	0.007	0.007	0.008
Si	0.003	0.004	0.006	0.004	0.005	0.026	0.004	0.007	0.004
Σ	1.000	1.000	1.000	1.000	1.000	1.000	1.000	1.000	1.000
M Site									
Al	0.691	0.675	0.757	0.792	0.751	0.743	0.736	0.664	0.657
Fe^{2+}	0.052	0.019	0.020	0.046	0.048	0.011	0.045	0.044	0.043
Fe^{3+}	0.084	0.108	0.164	0.136	0.161	0.170	0.152	0.199	0.188
Mg	0.021	0.022	0.031	0.007	0.001	0.055	0.027	0.009	0.008
Cr	1.138	1.160	1.012	1.002	1.020	1.005	1.022	1.071	1.090
Ti	0.010	0.012	0.016	0.013	0.014	0.014	0.014	0.010	0.010
Ni	0.004	0.003	0.000	0.004	0.004	0.003	0.004	0.003	0.004
Σ	2.000	2.000	2.000	2.000	2.000	2.000	2.000	2.000	2.000
Cr#	0.62	0.63	0.57	0.56	0.58	0.59	0.53	0.61	0.62
Mg#	0.57	0.57	0.46	0.47	0.52	0.51	0.53	0.47	0.47